One-Dimensional High-Q Silicon Nanoparticle Chain Resonators for Refractive Index Sensing

Lu Ding[†,*], Damien Eschimese[†], Thomas Ang[‡], Dmitry Morits[†], Hong Son Chu[‡], Soon Thor Lim[‡], Ching Eng Png[‡], Sergey Gorelik[†], Ramon Paniagua-Dominguez[†], and Arseniy I. Kuznetsov[†,*]

[†]*Institute of Materials Research and Engineering, A*STAR (Agency for Science, Technology and Research), 138634, Singapore*

[‡]*Institute of High Performance Computing, A*STAR (Agency for Science, Technology and Research), 138632, Singapore*

ABSTRACT

Label-free optical biosensors using nanophotonic concepts have made substantial progress in the last few years due to their ability to realize fast, compact and cost-effective chemical detection devices. Among those, high refractive index dielectric Mie nanoresonators hold promise for deep miniaturization of bio-sensing devices while keeping high sensitivity and low dissipative losses. In this work, we report a high sensitivity and small footprint refractive index sensor based on this concept. The device consists of a one-dimensional chain of coupled silicon nanoresonators supporting high quality factor collective Mie modes. The measurements with aqueous glycerol solutions show a high sensitivity range of 420 – 440 nm/RIU and a maximum figure of merit of 2700 RIU^{-1}. Being fully compatible with standard CMOS processes and having a small sensing area of only 0.5×18.2 μm^2, we believe this design, once arranged in arrays functionalized for different analytes, could become an attractive solution to realize lab-on-a-chip sensor arrays for high-performance, label-free multiplexing in a cost-effective way.

KEYWORDS: optical sensor, refractive index sensing, dielectric nanoantenna, resonant nanocavity, silicon photonics

INTRODUCTION

Nowadays, the usages and needs of chemical sensors and biosensors are continually increasing in modern societies to secure human health and well-being. Their applications range widely from food and environment contaminat detection to novel point-of-care medical diagnostics. Label-free optical sensing schemes based on nanoplasmonic[1] and nanophotonic[2] technologies have gained particular interest due to miniaturized footprint, high sensitivity, biocompatibility, and simultaneous real-time monitoring capabilities. The operation principle of the vast majority of optical sensors is based on refractive index sensing. Namely, the optical resonance mode of the sensing body is exposed to the environment and its peak position has one-to-one correspondence with the refractive index of the surrounding medium. There are two characteristic parameters to compare the refractive index sensors, namely the sensitivity and the so-called figure of merit[3]. The sensitivity (S) is defined as the shift of resonance frequency upon a change in the refractive index of the surrounding medium, *i.e.* $S = \Delta\lambda/\Delta n$. Large S is typically achieved in waveguide-based sensors, *e.g.* surface plasmon resonance (SPR) sensors[4-6], by increasing the overlap area between the analyte and the sensing body. These sensors are bulky and require a large amount of analyte. Another way to boost S is to utilize optical Vernier effect[7] in two coupled interferometers[8-9]. This method also increases the device footprint as well as the complexity of the sensor design. On the other hand, the figure of merit (FoM) is defined as the sensitivity (S) normalized by the full width at half maximum (FWHM) of the resonance mode, *i.e.* FoM = S/FWHM. The FoM defines the detection limits of localized refractive index change and gives a good quantitative measure of the

performance of resonator-based miniaturized sensors for surface refractive index sensing or biomolecule detection.

Plasmonic nanoantennas[10-13] with localized surface plasmon resonances (LSPR) are well known to sense the refractive index changes in their near field limited to a few tens of nanometers[14]. It enables foorprint miniaturization of the sensors and cost-effective devices. Besides that, LSPR sensors are able to resolve even single-molecule binding event on the surface of individual metal nanoparticles[15-17]. However, due to the Ohmic losses inherent to plasmonic nanoparticles at optical frequencies,[18] LSPR sensors suffer from low FoM and optical heating of the metallic nanoparticles and their surroundings, resulting in photothermal degradation of the sensor as well as the analyte[19]. Recently, high refractive index dielectric nanoantennas[20-21] have been found to be a suitable substitution of metallic counterparts for sensing applications[3, 22-26]. Dielectric nanoantennas support Mie-type electric and magnetic resonances in the subwavelength regime and have low dissipative losses and optical heating[27]. Resonance peak position from randomly distributed dielectric nanoantennas is also found to have a more linear response to adsorbate layer thickness changes[19]. However, the FoM of an individual dielectric nanoantenna is still generally low, below 10 per refractive index unit (RIU^{-1}) due to the broad resonance spectral linewidth. To improve the FoM, engineering of complex resonant structures with high quality factor is required. Nanoantenna arrays exhibiting spatially extended resonance features, such as Fano resonances[28], lattice resonances[22], supercavity modes[29], and bound states in the continuum[24], have improved FoMs to a few tens or even a few hundred RIU^{-1}.

Recently, we have reported a one-dimensional (1D) resonator composed of a chain of coupled silicon nanoantennas with a high quality factor resonance of up to 10^4 and high sensitivity to optical modulation[30]. Remarkably, these nanoresonators can be fabricated using conventional

photolithography processes in a cheap and scalable manner. Here, we show that the application of this kind of coupled Mie resonators to refractive index sensing allows us to achieve a sensor with an average sensitivity of 430 nm/RIU and the maximum FoM of 2700 RIU^{-1}. This finding result is much higher than what was previously shown for LSPR- and Mie resonance-based sensors and is comparable to the larger-scale sensors based on 1D photonic crystal cavities[31-36], subwavelength grating microring resonators[37], and suspended slot 2D photonic crystal cavities[38-39], which typically require more sophisticated and non-scalable nanofabrication procedures using electron beam lithography. Considering the compact footprint and possibility for large scale CMOS nanofabrication, on-chip sensor arrays based on 1D nanoparticle chain resonators would have great potential for realizing label-free sensing multiplexing in a cost-effective manner.

EXPERIMENTAL DETAILS

Numerical Design. 1D nanoparticle resonator for sensing is designed by adopting the same design rule as in our previous work[30]. The cavity consists of a chain of Mie-resonant nanoparticles with varied dimensions sandwiched between two similar nanoparticle chains with a photonic bandgap at the wavelength of operation and acting as highly reflective mirrors. The cavity resonance lies inside this photonic band gap opening a narrow transmission window. Figure 1a illustrates a schematic of the 1D nanoparticle resonator composed of 40 cuboidal silicon nanoparticles with identical height (H) of 220 nm, width (W) of 455 nm, period (Λ) of 455 nm and varied length. The whole system sits on SiO_2 (n = 1.45) and is immersed in water, which acts as a top cladding with a refractive index of 1.317 at 1550 nm wavelength[40]. The design length (L) of the mirror and cavity nanoparticles corresponding to their index numbers is shown as the solid grey curve in Figure 1b. Parabolic modulation of the length profile helps to provide a high quality factor of the cavity resonance[41]. FDTD simulation (see Methods) of light transmission through the resonant cavity

normalized to the source power is shown in Figure 1c. The aspect ratio of the nanoparticles (H/W) determines the polarization of the fundamental cavity resonance mode, corresponding to a linearly-polarized field transverse to the chain axis (TE_x). The lowest transmission band appears above 1543 nm with a maximum transmittance of 60% and a sharp resonance in the photonic bandgap at 1521.85 nm with a quality factor of ~7100. The effective mode volume is calculated to be ~ $1.12(\lambda/n_{Si})^3$, which is similar to the mode volume of 1D photonic crystal nanobeam cavities (typically ~$1(\lambda/n_{Si})^3$)[42]. At the cavity resonance, the nanoparticles support electric dipole modes (magnitude of the electric and magnetic field is shown in the insets of Figure 1c), which is advantageous for biomolecular sensing performance due to the higher exposure of the field to the surrounding medium[25]. All these make the nanoparticle chain resonator a suitable candidate for sensing applications.

Device Fabrication and Characterization. Figure 2a illustrates a schematic of the sensing device. The nanochain resonator is fabricated on a standard SOI chip with a 220 nm layer of crystalline silicon on top of a 2 μm SiO_2 cladding on a 500 μm silicon substrate (see Methods). The resonator, as the primary sensing body, is exposed to air or sensing liquid by selectively opening a sensing window, while coupling waveguides are protected by a top SiO_2 cladding. Figures 2b and 2c show the overview and zoom-in view of the scanning electron microscope (SEM) micrograph of the etched pattern. The resonator particles have the same width as the single mode silicon waveguides, which are used to couple light in and out of the resonator. The cuboidal shape of the nanoparticles is nicely reproduced, with slightly rounded corners, and the measured lengths (L) matches well the design, as shown in Figure 1b (black circles together with the measurement error). The transmission of the device is characterized by a tunable laser source and a photodetector (see Methods). Figure 2d plots the normalized transmission spectrum of the resonance when the cavity

is embedded in a DI water droplet. The resonance shows a clear Lorentzian profile and peaks at 1509.66 nm, with a quality factor of ~7500, which matches well with the simulations. The measured peak position is about 10 nm blue-shifted comparing to the simulated value, which we attribute to a slight deviation of the actual refractive index of silicon from the simulated one and fabrication imperfections.

RESULTS AND DISCUSSION

Covering the nanoparticle chain resonator with different refractive index materials leads to an expected shift of the cavity resonance. The characterization of the sensing response of the device is carried out by measuring the transmission spectrum of the cavity resonance when the sensor is drop-casted by glycerol – DI water mixture at various volume fractions V% of glycerol (Fig. S2). Between each step, the sensor is flushed thoroughly by running DI water and blow dried. The laser power is kept to a minimum to avoid any thermo-optic effect. The resonance of the cavity covered with DI water is used as the reference for calibration after each complete set of measurements. This helps to exclude any influence of variations of incidental factors (*e.g.* temperature variation). The normalized cavity resonance red shifts with increasing V% as shown in Figure 3a. The peak position of the resonance is extracted from the spectrum, and relative peak shift is plotted in Figure 3b as a function of refractive indices of the glycerol – DI water mixtures[38] at 1550 nm and 298 K. V% varies from 0% to 100% with a step of 10% and the refractive index monotonically increases from 1.3164 to 1.4569 with a nearly linear increment of 0.0147, correspondingly. Numerical simulations are also carried out to reproduce the peak shift as a function of refractive indices and the result is superimposed in Figure 3b (See Methods). Both measured and simulated peak shifts show similar near-linear growth, while the measured one has a slightly smaller slope indicating a smaller sensitivity. The actual sensitivity of the optical sensor relies on the local electromagnetic

filed distribution of the actual device. We attribute the discrepancy between the experiment and simulation to the fabrication inperfections and deviation of the actual refractive index of materials from the simulated values.

Figure 3c plots the sensor sensitivity $S = \Delta\lambda/\Delta n$, *i.e.,* the slope or local derivative of the peak shift with respect to the refractive index. The experimental value is in the range of 420 – 440 nm/RIU, while the simulation predicts one between 468 – 483 nm/RIU. The overall performance of the nanoparticle chain cavity sensor is then characterized by the figure of merit (FoM = S/FWHM). Figure 3d plots FoM depending on the refractive index of the local environment. The experiment FWHM of the resonance, obtained by Lorentzian fitting, gradually decreases from 202 pm to 168 pm with increasing refractive index. As a result, FoM has a gentle increase from 1900 to 2700 RIU^{-1}. These large FoM values, obtained for solutions with the refractive index in the range of 1.31 to 1.4, which corresponds to the typical refractive index values for most biomaterials[43], validate the good performance of our device. We note that the obtained S and FoM values are comparable to the best sensors based on 1D photonic crystal cavities[33-35] but can be achieved here in more compact structures, which also can be fabricated with simpler and scalable CMOS nanofabrication techniques[30].

Table 1 List of state-of-the-art 1D photonic sensing structures with their key parameters. PCNBC and PCC are the acronyms of photonic crystal nanobeam cavity and photonic crystal cavity, respectively.

Configuration	**Materials**	**RI Range**	**Footprint** μm^2	**Mode Volume**	**Sensitivity** nm/RIU	**FoM** RIU^{-1}
PCC[33]	SOI	$\Delta n = 0.03$	2×16	$1.48(\lambda/n_{Si})^3$	269	4638
Slotted PCC[34]	SOI	1.333*-1.378	2.5×16.8	$0.217(\lambda/n_{Si})^3$	410	1213
PCC[35]	SOI	1.333*-1.378	0.75×14.6	$1.28(\lambda/n_{Si})^3$	428	3590
Suspended coupled PCNBC[31]	InGaAsP	1.333*,1.342	1.1×12.7	--	900	419
PCNBC[32]	Polymer	--	3.2×110	$\sim 30(\lambda/n_{ZEP})^3$	386	9190
quadrabeam PCC[44]	SOI	1.333*-1.3658	1.1×29	--	451	2060
Porous PCNBC[36]	Porous-Si	$\Delta n = 0.03$	1.2×20	--	1000	842
Our device	SOI	1.316[40]-1.457	0.5×18.2	$1.12(\lambda/n_{Si})^3$	430	2700

* It is worth mentioning that the refractive index of water of 1.333[45] used in all the listed works is the value taken at 556 nm and 289 K while the typical detection wavelength is around 1550 nm. Rigorously, the refractive index of water of 1.3164[40] must be used instead. It might slightly alter the reported sensitivity.

To make a proper comparison of our sensor to the other state-of-the-art 1D photonic sensing structures such as photonic crystal nanobeam cavity (PCNBC) and photonic crystal cavity (PCC), we summarize the key obtained parameters in Table 1. As can be seen from this comparison, our sensor has the smallest device footprint ($0.5\times18.2\ \mu m^2$) comparing to all the listed sensors while keeping the high performance. Importantly, our sensor is also based on SOI platform with CMOS fabrication compatibility, miniaturization, and integration. The refractive index range of operation is adjusted for water-based solutions that cover liquid environment of most of biomaterials. Thus, our compact structure is attractive for realizing on-chip sensor arrays for label-free multiplexing. Combining with microfluidic channels, the device has strong potential for lab-on-a-chip applications[2, 46].

CONCLUSIONS

In this paper, we have demonstrated a high-performance refractive index sensor based on 1D resonator formed by a chain of coupled silicon nanoantennas. The average sensitivity of 430 nm/RIU and maximum FoM of 2700 RIU^{-1} are measured for the refractive index range of 1.3 to 1.4. Our sensor significantly outperforms other sensors made from an individual dielectric nanoantenna due to the high quality factor of the cavity resonance. In addition, the sensor is highly compact with a footprint of only $0.5\times18.2\ \mu m^2$, and the width of the sensor is no greater than a silicon single mode waveguide. The demonstrated device has high Q-factor, large FoM, wide sensing range and small sensing area. It will be a promising candidate to realize on-chip sensor arrays for label-free multiplexing. We also highlight the potential of this design to realize cost-effective devices, as wafer-level fabrication of similar chain resonators has already been realized using CMOS compatible photolithography[30].

REFERENCES

(1) Soler, M.; Huertas, C. S.; Lechuga, L. M., Label-free plasmonic biosensors for point-of-care diagnostics: a review. *Expert Rev. Mol. Diagn.* **2019,** *19* (1), 71-81.

(2) Luan, E.; Shoman, H.; Ratner, D.; Cheung, K.; Chrostowski, L., Silicon photonic biosensors using label-free detection. *Sensors* **2018,** *18* (10), 3519.

(3) Krasnok, A.; Caldarola, M.; Bonod, N.; Alú, A., Spectroscopy and biosensing with optically resonant dielectric nanostructures. *Adv. Opt. Mater.* **2018,** *6* (5), 1701094.

(4) Gartia, M. R.; Hsiao, A.; Pokhriyal, A.; Seo, S.; Kulsharova, G.; Cunningham, B. T.; Bond, T. C.; Liu, G. L., Colorimetric plasmon resonance imaging using nano lycurgus cup arrays. *Adv. Opt. Mater.* **2013,** *1* (1), 68-76.

(5) Chen, Z.; Liu, L.; He, Y.; Ma, H., Resolution enhancement of surface plasmon resonance sensors with spectral interrogation: resonant wavelength considerations. *Appl. Opt.* **2016,** *55* (4), 884-891.

(6) Yavas, O.; Acimovic, S. S.; Garcia-Guirado, J.; Berthelot, J.; Dobosz, P.; Sanz, V.; Quidant, R., Self-calibrating on-chip localized surface plasmon resonance sensing for quantitative and multiplexed detection of cancer markers in human serum. *ACS sensors* **2018,** *3* (7), 1376-1384.

(7) Gomes, A. D.; Bartelt, H.; Frazão, O., Optical Vernier Effect: Recent Advances and Developments. *Laser Photonics Rev.* **2021**, 2000588.

(8) Claes, T.; Bogaerts, W.; Bienstman, P., Experimental characterization of a silicon photonic biosensor consisting of two cascaded ring resonators based on the Vernier-effect and introduction of a curve fitting method for an improved detection limit. *Opt. Express* **2010,** *18* (22), 22747-22761.

(9) Gomes, A. D.; Kobelke, J.; Bierlich, J.; Dellith, J.; Rothhardt, M.; Bartelt, H.; Frazão, O., Giant refractometric sensitivity by combining extreme optical Vernier effect and modal interference. *Sci. Rep.* **2020,** *10* (1), 1-14.

(10) Kuznetsov, A. I.; Evlyukhin, A. B.; Gonçalves, M. R.; Reinhardt, C.; Koroleva, A.; Arnedillo, M. L.; Kiyan, R.; Marti, O.; Chichkov, B. N., Laser fabrication of large-scale nanoparticle arrays for sensing applications. *ACS nano* **2011,** *5* (6), 4843-4849.

(11) Offermans, P.; Schaafsma, M. C.; Rodriguez, S. R.; Zhang, Y.; Crego-Calama, M.; Brongersma, S. H.; Gómez Rivas, J., Universal scaling of the figure of merit of plasmonic sensors. *ACS nano* **2011,** *5* (6), 5151-5157.

(12) Cao, G.; Li, H.; Deng, Y.; Zhan, S.; He, Z.; Li, B., Systematic theoretical analysis of selective-mode plasmonic filter based on aperture-side-coupled slot cavity. *Plasmonics* **2014,** *9* (5), 1163-1169.

(13) Deng, Y.; Cao, G.; Wu, Y.; Zhou, X.; Liao, W., Theoretical description of dynamic transmission characteristics in MDM waveguide aperture-side-coupled with ring cavity. *Plasmonics* **2015,** *10* (6), 1537-1543.

(14) Acimovic, S. S.; Kreuzer, M. P.; González, M. U.; Quidant, R., Plasmon near-field coupling in metal dimers as a step toward single-molecule sensing. *ACS nano* **2009,** *3* (5), 1231-1237.

(15) Mayer, K. M.; Hao, F.; Lee, S.; Nordlander, P.; Hafner, J. H., A single molecule immunoassay by localized surface plasmon resonance. *Nanotechnology* **2010,** *21* (25), 255503.

(16) Zijlstra, P.; Paulo, P. M.; Orrit, M., Optical detection of single non-absorbing molecules using the surface plasmon resonance of a gold nanorod. *Nat. Nanotechnol.* **2012,** *7* (6), 379-382.

(17) Aćimović, S. S.; Šípová-Jungová, H.; Emilsson, G.; Shao, L.; Dahlin, A. B.; Käll, M.; Antosiewicz, T. J., Antibody–antigen interaction dynamics revealed by analysis of single-molecule equilibrium fluctuations on individual plasmonic nanoparticle biosensors. *Acs Nano* **2018,** *12* (10), 9958-9965.

(18) Khurgin, J. B., How to deal with the loss in plasmonics and metamaterials. *Nat. Nanotechnol.* **2015,** *10* (1), 2-6.

(19) Bosio, N.; Šípová-Jungová, H.; Länk, N. O.; Antosiewicz, T. J.; Verre, R.; Käll, M., Plasmonic versus all-dielectric nanoantennas for refractometric sensing: A direct comparison. *Acs Photonics* **2019,** *6* (6), 1556-1564.
(20) Kuznetsov, A. I.; Miroshnichenko, A. E.; Fu, Y. H.; Zhang, J.; Luk'Yanchuk, B., Magnetic light. *Sci. Rep.* **2012,** *2*, 492.
(21) Kuznetsov, A. I.; Miroshnichenko, A. E.; Brongersma, M. L.; Kivshar, Y. S.; Luk'yanchuk, B., Optically resonant dielectric nanostructures. *Science* **2016,** *354* (6314), aag2472.
(22) Yavas, O.; Svedendahl, M.; Dobosz, P.; Sanz, V.; Quidant, R., On-a-chip biosensing based on all-dielectric nanoresonators. *Nano letters* **2017,** *17* (7), 4421-4426.
(23) Bontempi, N.; Chong, K. E.; Orton, H. W.; Staude, I.; Choi, D.-Y.; Alessandri, I.; Kivshar, Y. S.; Neshev, D. N., Highly sensitive biosensors based on all-dielectric nanoresonators. *Nanoscale* **2017,** *9* (15), 4972-4980.
(24) Romano, S.; Zito, G.; Torino, S.; Calafiore, G.; Penzo, E.; Coppola, G.; Cabrini, S.; Rendina, I.; Mocella, V., Label-free sensing of ultralow-weight molecules with all-dielectric metasurfaces supporting bound states in the continuum. *Photonics Res.* **2018,** *6* (7), 726-733.
(25) Yavas, O.; Svedendahl, M.; Quidant, R., Unravelling the role of electric and magnetic dipoles in biosensing with Si nanoresonators. *ACS nano* **2019,** *13* (4), 4582-4588.
(26) Aoni, R. A.; Manjunath, S.; Karawdeniya, B. I.; Zangeneh Kamali, K.; Xu, L.; Damry, A. M.; Jackson, C. J.; Tricoli, A.; Miroshnichenko, A. E.; Rahmani, M., Resonant Dielectric Metagratings for Response Intensified Optical Sensing. *Adv. Funct. Mater.* **2021**, 2103143.
(27) Caldarola, M.; Albella, P.; Cortés, E.; Rahmani, M.; Roschuk, T.; Grinblat, G.; Oulton, R. F.; Bragas, A. V.; Maier, S. A., Non-plasmonic nanoantennas for surface enhanced spectroscopies with ultra-low heat conversion. *Nat. Commun.* **2015,** *6* (1), 1-8.
(28) Chong, K. E.; Orton, H. W.; Staude, I.; Decker, M.; Miroshnichenko, A. E.; Brener, I.; Kivshar, Y. S.; Neshev, D. N., Refractive index sensing with Fano resonances in silicon oligomers. *Philos. Trans. R. Soc. A* **2017,** *375* (2090), 20160070.
(29) Tittl, A.; Leitis, A.; Liu, M.; Yesilkoy, F.; Choi, D.-Y.; Neshev, D. N.; Kivshar, Y. S.; Altug, H., Imaging-based molecular barcoding with pixelated dielectric metasurfaces. *Science* **2018,** *360* (6393), 1105-1109.
(30) Ding, L.; Morits, D.; Bakker, R.; Li, S.; Eschimese, D.; Zhu, S.; Yu, Y. F.; Paniagua-Dominguez, R.; Kuznetsov, A. I., All-Optical Modulation in Chains of Silicon Nanoantennas. *ACS Photonics* **2020,** *7* (4), 1001-1008.
(31) Wang, B.; Dündar, M. A.; Nötzel, R.; Karouta, F.; He, S.; van der Heijden, R. W., Photonic crystal slot nanobeam slow light waveguides for refractive index sensing. *Appl. Phys. Lett.* **2010,** *97* (15), 151105.
(32) Quan, Q.; Burgess, I. B.; Tang, S. K.; Floyd, D. L.; Loncar, M., High-Q, low index-contrast polymeric photonic crystal nanobeam cavities. *Opt. Express* **2011,** *19* (22), 22191-22197.
(33) Yao, K.; Shi, Y., High-Q width modulated photonic crystal stack mode-gap cavity and its application to refractive index sensing. *Opt. Express* **2012,** *20* (24), 27039-27044.
(34) Xu, P.; Yao, K.; Zheng, J.; Guan, X.; Shi, Y., Slotted photonic crystal nanobeam cavity with parabolic modulated width stack for refractive index sensing. *Opt. Express* **2013,** *21* (22), 26908-26913.
(35) Zhang, Y.; Han, S.; Zhang, S.; Liu, P.; Shi, Y., High-Q and high-sensitivity photonic crystal cavity sensor. *IEEE Photonics J.* **2015,** *7* (5), 1-6.
(36) Rodriguez, G. A.; Markov, P.; Cartwright, A. P.; Choudhury, M. H.; Afzal, F. O.; Cao, T.; Halimi, S. I.; Retterer, S. T.; Kravchenko, I. I.; Weiss, S. M., Photonic crystal nanobeam biosensors based on porous silicon. *Opt. Express* **2019,** *27* (7), 9536-9549.
(37) Yan, H.; Huang, L.; Xu, X.; Chakravarty, S.; Tang, N.; Tian, H.; Chen, R. T., Unique surface sensing property and enhanced sensitivity in microring resonator biosensors based on subwavelength grating waveguides. *Opt. Express* **2016,** *24* (26), 29724-29733.
(38) Di Falco, A.; O'faolain, L.; Krauss, T., Chemical sensing in slotted photonic crystal heterostructure cavities. *Appl. Phys. Lett.* **2009,** *94* (6), 063503.

(39) Jágerská, J.; Zhang, H.; Diao, Z.; Le Thomas, N.; Houdré, R., Refractive index sensing with an air-slot photonic crystal nanocavity. *Opt. Lett.* **2010,** *35* (15), 2523-2525.
(40) Saunders, J. E.; Sanders, C.; Chen, H.; Loock, H.-P., Refractive indices of common solvents and solutions at 1550 nm. *Appl. Opt.* **2016,** *55* (4), 947-953.
(41) Desiatov, B.; Goykhman, I.; Levy, U., Parabolic tapered photonic crystal cavity in silicon. *Appl. Phys. Lett.* **2012,** *100* (4), 041112.
(42) Kuramochi, E.; Taniyama, H.; Tanabe, T.; Kawasaki, K.; Roh, Y.-G.; Notomi, M., Ultrahigh-Q one-dimensional photonic crystal nanocavities with modulated mode-gap barriers on SiO_2 claddings and on air claddings. *Opt. Express* **2010,** *18* (15), 15859-15869.
(43) Patel, S. K.; Parmar, J.; Sorathiya, V.; Nguyen, T. K.; Dhasarathan, V., Tunable infrared metamaterial-based biosensor for detection of hemoglobin and urine using phase change material. *Sci. Rep.* **2021,** *11* (1), 1-11.
(44) Yang, D.; Kita, S.; Liang, F.; Wang, C.; Tian, H.; Ji, Y.; Lončar, M.; Quan, Q., High sensitivity and high Q-factor nanoslotted parallel quadrabeam photonic crystal cavity for real-time and label-free sensing. *Appl. Phys. Lett.* **2014,** *105* (6), 063118.
(45) Palmer, K. F.; Williams, D., Optical properties of water in the near infrared. *J. Opt. Soc. Am. B* **1974,** *64* (8), 1107-1110.
(46) Barrios, C. A., Integrated microring resonator sensor arrays for labs-on-chips. *Anal. Bioanal. Chem.* **2012,** *403* (6), 1467-1475.

Methods

Numerical Simulation: Finite difference time domain (FDTD) method was employed to calculate the resonance spectrum of the chain of nanoparticles embedded in water-glycerol mixture with different glycerol concentration using commercial software (Lumerical FDTD). The 1D nanoparticle chain resonator system consisting of 40 cuboidal silicon nanoparticles with identical height (H) of 220nm, width (W) of 455nm and period (Λ) of 455nm was simulated. Silicon strip waveguides of the same H and W dimensions are used as input and output for the coupling to and collection of light from the resonator system. The simulation domain consists of the input and output silicon waveguides, and the 1D nanoparticle chain resonator system sitting on top of SiO_2 cladding with a refractive index of 1.45 and with top cladding with varied refractive index. Perfectly matched layer (PML) boundary conditions were used to surround the whole system. Transverse electric (TE) polarization, in which the dominant electric field is polarized horizontally, is chosen to match with the modes of the waveguide and cavity. The 3D silicon strip waveguide mode is injected into the input waveguide, transmitted through the 1D resonator chain, and exits through the output waveguide. Appropriate monitors are placed to record the transmission by normalizing the output power with the input source power. Simulations were performed for different glycerol concentration (0 to 100%) and compared with the experimental results.

Fabrication: Devices are fabricated by EBL on a blank SOI chip (20×20 mm^2) with 220 nm of crystalline silicon on top of a 2 µm SiO_2 layer on the 500 µm silicon substrate using the same process described previously[30]. There, we have also demonstrated that similar structures based on the same materials can be obtained using conventional 8-inch CMOS photolithography processes. After etching, the nanoparticle chain cavity was protected by solid PDMS film and the whole structure was covered by a top SiO_2 cladding with a thickness of 2.5 µm using ICP chemical vapor

deposition (Plasmalab System 100, Oxford). The chip was manually cleaved and the facets were mechanically polished to the end of the edge couplers which are composed of inverse taper waveguides. PDMS film was then peeled off to expose the cavity window for refractive index sensing.

Transmission characterization: An image of transmission measurement set-up is shown in Fig. S3. The characterization method is the same as described previously[30].

SUPPORTING INFORMATION

Measurement procedure, glycerol preparation procedure, and transmission measurement set-up.

AUTHOR INFORMATION

*Corresponding Authors, E-mail: Arseniy_Kuznetsov@imre.a-star.edu.sg and dingl@imre.a-star.edu.sg

AUTHOR CONTRIBUTIONS

L.D. performed optical characterizations, analyzed data, and wrote the first draft of the manuscript. D.E. fabricated the sample and performed SEM. D.M. and R.P.D. performed simulations on SiO_2 embedded chain resonators. T.A. performed simulations on resonators covered by water-glycerol mixture. L.D. and S.G. prepared water-glycerol mixture. A.I.K. proposed the initial concept and supervised the work. All authors contributed to writing the manuscript.

ACKNOWLEDGEMENT

This work was supported by A*STAR SERC Pharos program, Grant No. 152 73 00025 (Singapore).

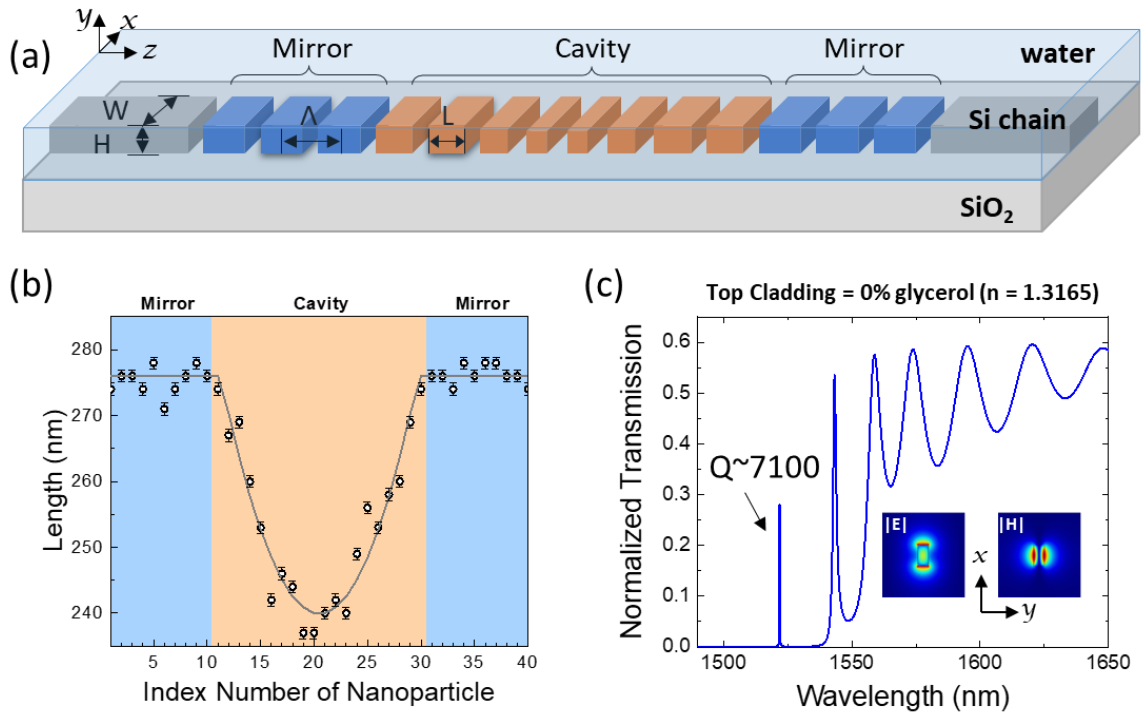

Figure 1 (a) Schematics of the 1D silicon nanoparticle chain resonator with top and bottom claddings. (b) Length profile of the mirror and cavity nanoparticles: grey solid curve is used in numerical simulations; black circles are taken from experiment. (c) FDTD simulation of transmittance through the resonant cavity and input/output waveguide with bottom SiO_2 cladding and top water cladding. Inset shows electric and magnetic field profile, |E| and |H|, of the nanoparticle's resonance mode in x-y plane.

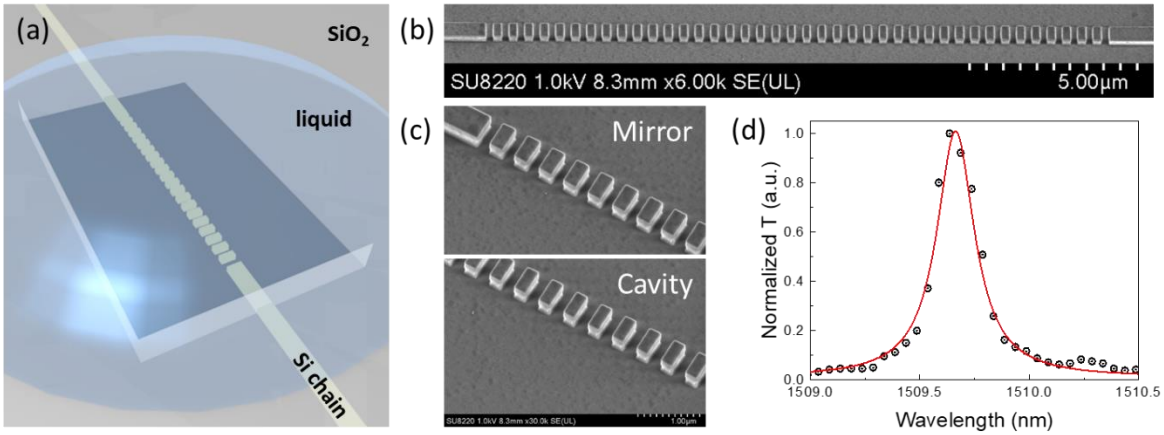

Figure 2 (a) Artistic illustration of the sensing device where the chain resonator is exposed to drop-casted liquid environment. (b) and (c) Scanning electron microscope (SEM) images of the nanoparticle chain resonator. (d) Experiment transmission spectrum of the cavity immersed in DI water at the resonance normalized by its peak transmission.

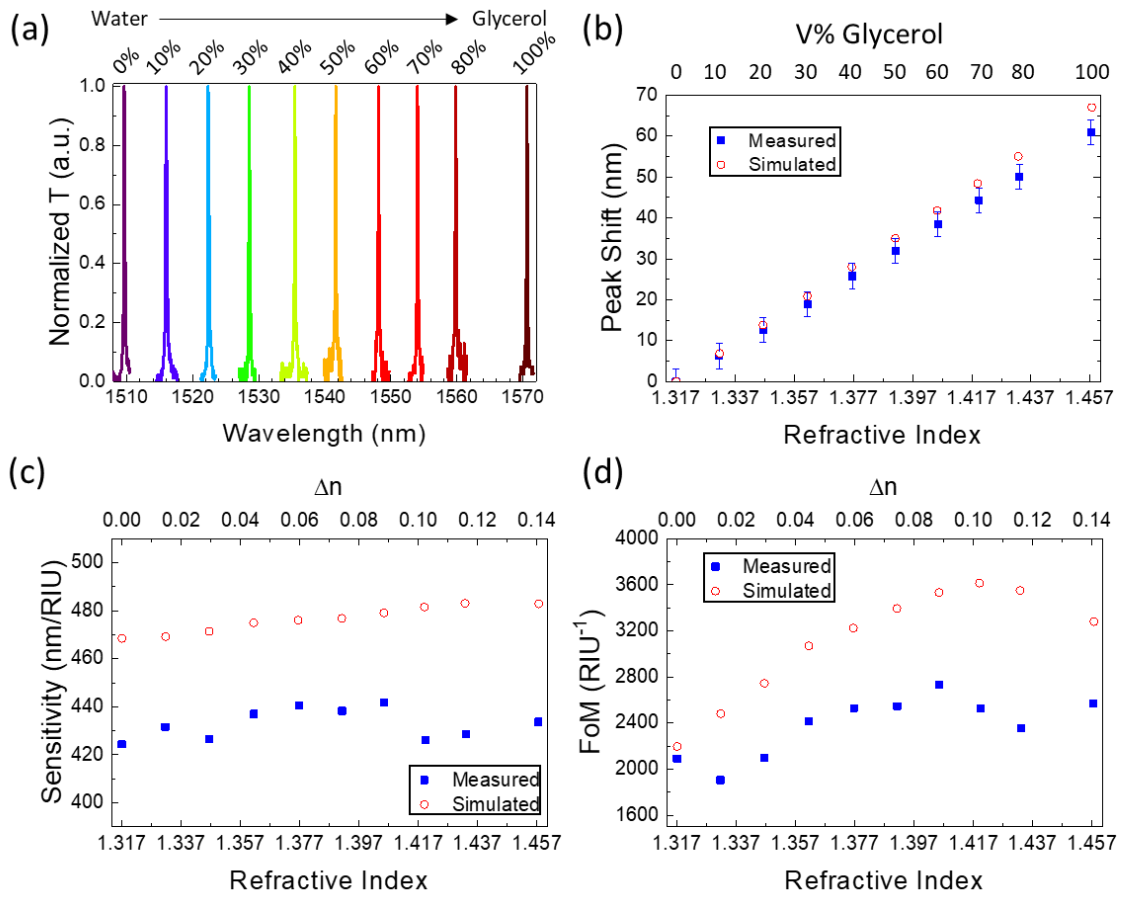

Figure 3 (a) Resonance spectra as a function of volume fraction V% of glycerol in DI water. (b) Measured and simulated peak shift of the cavity resonance vs. glycerol concentration and refractive index of the mixture at room temperature and 1550 nm[40]. The error bar shows the peak position variation in different repetitive measurements (Fig. S1). Measured and simulated sensitivity (c) and FoM (d) as a function of the refractive index.

TOC Graphic

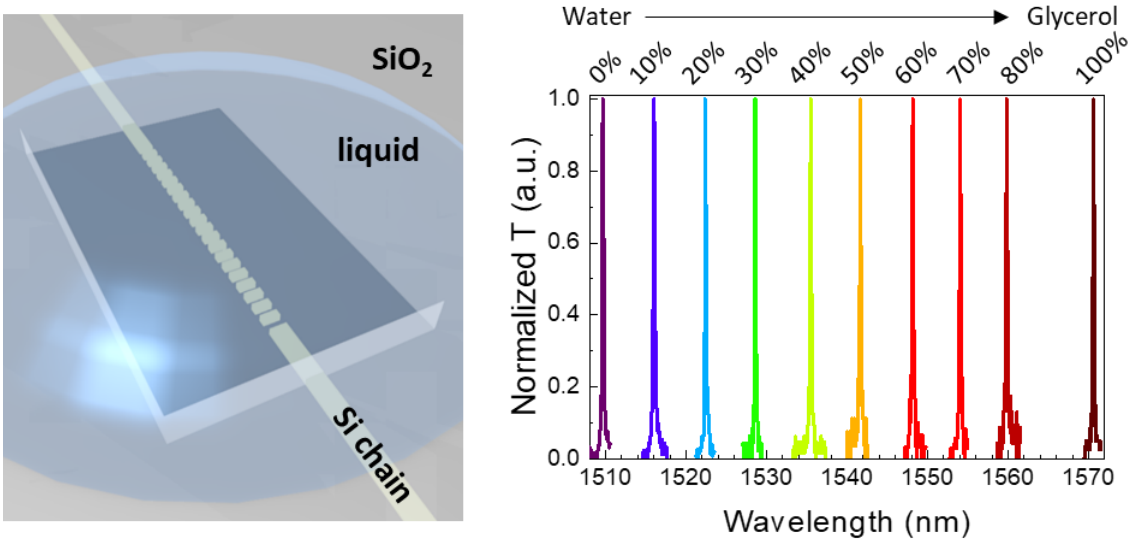
SiO2
liquid
Si chain
Water
Glycerol
0%
10%
20%
30%
40%
50%
60%
70%
80%
100%
Normalized T (a.u.)
1.0
0.8
0.6
0.4
0.2
0.0
1510
1520
1530
1540
1550
1560
1570
Wavelength (nm)